Journal of Membrane Science 598 (2020) 117665

Contents lists available at ScienceDirect

Journal of Membrane Science

journal homepage: http://www.elsevier.com/locate/memsci

Poly(terphenylene) anion exchange membranes with high conductivity and low vanadium permeability for vanadium redox flow batteries (VRFBs)

Tongshuai Wang [a], Jong Yeob Jeon [b], Junyoung Han [b], Jae Heon Kim [a,c], Chulsung Bae [b,**], Sangil Kim [a,*]

[a] Department of Chemical Engineering, University of Illinois at Chicago, Chicago, IL, 60607, USA
[b] Department of Chemistry & Chemical Biology, Rensselaer Polytechnic Institute, Troy, NY, 12180, USA
[c] New Trier High School, Winnetka, IL, 60093, USA

ARTICLE INFO

Keywords:
Anion exchange membrane
Vanadium redox flow battery
Selective ion transport

ABSTRACT

In this study, we demonstrate a new class of poly(terphenylene) based anion exchange membranes (AEMs) with improved chemical stability and anion conductivity in vanadium redox flow batteries (VRFBs). A series of terphenyl- and biphenyl-based polymers with pendant quaternary ammonium alkyl groups were synthesized and characterized for VRFB applications. When the arrangement of the polymer backbone and cation-tethered alkyl chains was varied, the prepared AEM membranes exhibited extremely low vanadium permeance while maintaining high conductivity. These properties further provided a high coulombic efficiency close to 100% at all current densities as well as high voltage efficiency. The single cell VRFB performance with the poly(terphenylene) based AEMs showed 2–5% higher coulombic efficiency than those of commercial AEMs and similar voltage efficiency to those of commercial PEMs (Nafion® 212). The highest EE value of 93.64% was achieved at the current density of 20 mA/cm^2 (vs. 72% EE for Nafion212). In addition, poly(terphenylene) based AEMs showed superior cycle stability and high capacity retention, thus demonstrating their high performance as promising IEMs for VRFB application.

1. Introduction

Driven by the ever-growing demand for electricity generated from green sources, redox flow batteries (RFBs) have received great attention for their potential for implementation in large-scale on-grid electric energy storage for integration with renewable energy [1,2]. Among the various available RFB technologies, vanadium redox flow batteries (VRFBs) have received the most attention, owing to their absence of and intercalation/deintercalation in electrodes and cross-contamination of electrolytes, facile heat management, safe operation, and long service life [3,4].

Because they are key components in VRFBs, many different types of ion exchange membranes (IEMs) have been extensively studied over the past decade. The essential characteristics of ideal IEMs for VRFBs can be summarized as follows: (1) low permeation rates of vanadium ions to minimize self-discharging and capacity fading (i.e., high columbic efficiency, CE); (2) high ion conductivity for the transport of charge-carrying ions (e.g., H^+ and SO_4^{2-}) to maintain the electric circuit (i.e., high voltage efficiency, VE); (3) low area-specific resistance to minimize efficiency loss caused by ohmic polarization; (4) excellent cycle stability; and (5) low manufacturing cost to enable commercialization [5,6].

To date, the most commonly used IEMs in VRFBs are perfluorinated proton exchange membranes (PEMs), such as DuPont's Nafion® and its derivatives, because of their excellent chemical stability and proton conductivity, which provide good cycle stability and high VE [7]. However, most PEMs have the drawback of severe vanadium crossover flow, which lowers the CE of battery stacks and causes faster capacity decay [8–10]. This issue is mainly due to the intrinsic affinity of PEMs for cationic species, which facilitate crossover of cationic vanadium ions (VO_2^+/V_3^+) along with charge carriers (protons) [11]. Although numerous efforts have been made to resolve these issues [12–16], the limitation of the trade-off between proton conductivity and proton/vanadium selectivity still remains [6].

To circumvent the above-mentioned problems of PEMs, anion

* Corresponding author.
** Corresponding author.
E-mail addresses: baec@rpi.edu (C. Bae), sikim@uic.edu (S. Kim).

https://doi.org/10.1016/j.memsci.2019.117665
Received 27 August 2019; Received in revised form 12 November 2019; Accepted 13 November 2019
Available online 15 November 2019

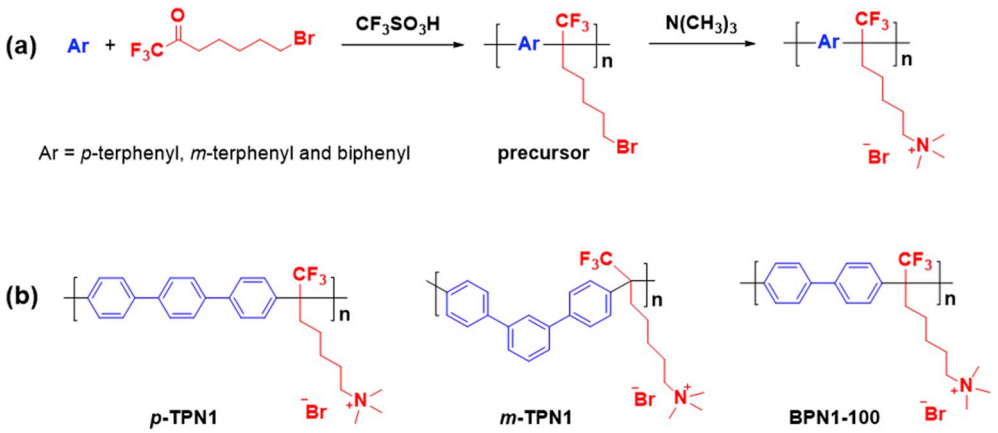

Fig. 1. (a) Synthetic route for *p*-TPN1, *m*-TPN1, and BPN1-100 and (b) their chemical structures.

exchange membranes (AEMs) have been proposed as a new solution in VRFB applications, which can effectively suppress cationic vanadium ions while being permeable to anionic charge carriers (e.g., SO_4^{2-}). As explained by the Donnan exclusion model, the equilibrium concentration of vanadium ions in AEM can be greatly restricted by the electrostatic repulsion of fixed cationic groups in IEM, and subsequently, AEMs can reject cationic vanadium species more effectively than PEMs [17], thus resulting in a higher CE. However, the major limitation of AEMs in VRFB applications is their unsatisfactory anion conductivity, which is considered to come from the low anion (e.g. SO_4^{2-}) mobility in the polymer matrix and aqueous electrolyte solution compared with proton mobility in same environment [18]. Moreover, another drawback of AEMs is their poor chemical stability in acidic and oxidative environments [19,20]. Among many efforts to improve anion conductivity and the chemical/mechanical stability of AEMs, quaternary ammonium functionalized AEMs have been most extensively studied, owing to their facile synthesis procedure and flexible design [18,19,21,22]. Recently, we developed a new class of terphenyl-based polymeric membranes with quaternary ammonium group terminated side chains, *p*-TPN1 (*para*--terphenyl) and *m*-TPN1 (*meta*-terphenyl), and demonstrated their high hydroxide anion conductivity as well as improved fuel cell performance [23]. The unique microstructure and morphology of these AEM significantly enhance anion conductivity, thus resulting in superior fuel cell performance. Nevertheless, the performance of these promising polymers in VRFB applications has not yet been studied.

In this study, we systematically investigated how molecular structures of poly(terphenylene)-based AEM (terphenyl-based *p*-TPN1 and *m*-TPN1) affected VRFB performance. In addition, we compared the results of terphenyl-based AEMs with biphenyl-based AEM (BPN1-100) to investigate the effects of polymer backbones on ion transport properties, electrochemical performance, and membrane stability. The *p*-TPN1 and *m*-TPN1 membranes exhibited orders of magnitude lower vanadium ion diffusivity and higher proton/vanadium ion selectivity (16.31 for *p*-TPN1 and 10.29 for *m*-TPN1) than commercial Nafion (0.58) and FAP-450 (0.81) membranes. Consequently, the VRFB with *p*-TPN1 showed an excellent energy efficiency (EE) of 86.07% at current density of 80 mA/cm^2, compared with ~78% for Nafion 212 and FAP-450.

2. Experimental section

2.1. Chemicals

Nafion® 117 and 212 were purchased from Ion Power Inc. (DE, USA). A commercial AEM, Fumasep® FAP-450, was purchased from FUMATECH BWT GmbH (Bietigheim-Bissingen, Germany). Vanadyl sulfate ($VOSO_4$, 99.9%) and magnesium sulfate ($MgSO_4$, 99.5%) were purchased from Alfa Aesar (MA, USA). Sulfuric acid (H_2SO_4, 98.0%) was purchased from Fisher Scientific (PA, USA). All reagents and solvents used for synthesis of the polymers were purchased from Aldrich, Alfa Aesar, TCI Chemical Co., and Strem Chemicals, and were used without further purification.

Table 1
Properties of precursor polymers.

Samples	Mn (kDa)	Mw (kDa)	PDI	DF (%)
p-TPBr	50	94	1.9	100
m-TPBr	41	126	3.1	100
BPBr-100	45	86	1.9	100

2.2. Polymer synthesis and characterization

p-TPN1, *m*-TPN1, and BPN1-100 were synthesized by acid-catalyzed Friedel-Crafts polycondensation of aromatic monomers and 7-bromo-1,1,1-trifluoroheptan-2-one, followed by quaternization of alkyl bromide with trimethylamine (Fig. 1a). The detailed synthetic methods have been described in our previous publications [23,24] and the chemical structures of the polymers are shown in Fig. 1b. The molecular structures were confirmed by ^{1}H NMR.

The polymers are alternating copolymers composed of aromatic unit (blue in Fig. 1b) and a trimethylammonium (TMA) group-tethered alkyl unit (red in Fig. 1b). The aromatic unit was varied by changing the aromatic monomers, *para*-terphenyl, *meta*-terphenyl and biphenyl for *p*-TPN1, *m*-TPN1 and BPN1-100, respectively. The insertion of a sp^3–hybridized tetrahedral carbon spacer between rigid aromatic groups on the polymer backbones enhances flexibility of the polymer chain, affording high molecular weights and excellent mechanical properties; the three AEMs show tensile stress higher than 20 MPa at 50 °C and 50% relative humidity condition [23,25].

The molecular weights of the polymers are measured from alkyl bromide-containing neutral precursor polymers instead of the quaternary ammonium-containing polymers. This is because the presence of ionic groups in the polymers tends to form polymer aggregates and results in complicated and unreliable molecular weight characterization in size exclusion chromatography (SEC) [26]. *p*-TPBr, *m*-TPBr and BPBr-100 are the precursor polymers of *p*-TPN1, *m*-TPN1 and BPN1-100, respectively, and their SEC results are listed in Table 1.

The number- and weight-average molecular weights of polymers were determined by SEC on a Viscotek T60A instrument with a differential refractive index detector (Viscotek 302), using THF as the eluent and polystyrene as the standard.

2.3. Membrane preparation

AEM membranes were prepared by casting 5–7 wt% polymer/DMSO solution on a homemade polypropylene/glass mold. The membranes were subsequently dried at 70 °C under a constant flow of nitrogen for 24 h to avoid contacting with moisture which can cause pores or pinholes in the membrane. Nafion® membranes were pretreated with 3 wt % H_2O_2 solution for 1 h, boiling deionized water for 1 h, and boiling 1 mol/L H_2SO_4 solution for 30 min [27]. Fumasep® FAP-450 membrane was used without any pre-treatment. All membrane samples were immersed in 1 M H_2SO_4 for 1 day before characterization and battery tests.

2.4. Ion exchange capacity (IEC)

The weight-based ion exchange capacity (IEC_w) of Nafion was measured through conventional titration methods [27]. The membrane samples were immersed in a 1 N NaCl solution for 24 h to substitute the H^+ ions of the sulfonic acid groups with Na^+ ions. The substituted solution was titrated with a 0.01 M NaOH solution with phenolphthalein as an indicator. The IEC_w value of PEMs ($IEC_{w,PEM}$) was calculated with the following equation:

$$IEC_{w,PEM} = \frac{0.01 \times V_{NaOH}}{W_{dry}}, \quad (1)$$

where V_{NaOH} is the volume of NaOH solution added in titration, and W_{dry} is the weight of the membrane in a dry state.

The ion exchange capacity for AEMs was measured by Mohr titration [23]. Approximately 0.15 g of membrane was dried at 50 °C in a vacuum for 24 h and weighed. The membrane in bromide form was immersed in 20 mL of a 0.1 M $NaNO_3$ solution for 48 h. The $NaNO_3$ solution was titrated with a 0.1 M $AgNO_3$ by using K_2CrO_4 as a colorimetric indicator. IEC was calculated from the dry mass of the membrane and the amount $AgNO_3$ consumed in titration.

The IEC_w value of AEMs ($IEC_{w,AEM}$) was calculated with the following equation:

$$IEC_{w,AEM} = \frac{0.1 \times V_{AgNO_3}}{W_{dry}} \quad (2)$$

where V_{AgNO_3} is the volume of $AgNO_3$ solution added in titration, and W_{dry} is the weight of the membrane in a dry state.

2.5. VO^{2+} permeability (P_{VO2+})

The vanadium permeability based on VO^{2+} ions has been commonly tested for membranes in VRFB applications due to the higher stability of VO^{2+} ions in air compared to other vanadium species [5,27,28]. A home-made diffusion cell composed of two half cells was used to perform the tests [29–32]. The prepared membrane with a testing area of 1.76 cm^2 was sandwiched between two diffusion half cells. One side reservoir was filled with 11 mL of $VOSO_4$ (1 M) in H_2SO_4 (2 M) solution, and another side reservoir was filled 11 mL of $MgSO_4$ (1 M) in H_2SO_4 (2 M) solution. A magnetic stirrer was placed in each diffusion cell to prevent concentration polarization. The concentration of the VO^{2+} ions was measured using UV–Vis spectroscopy (T7S, Persee Analytics, China). The VO^{2+} permeability through the membrane was calculated by:

$$V\frac{dC_B(t)}{dt} = A\frac{P}{L}(C_A - C_B(t)), \quad (3)$$

where V is the volume of solution in each reservoir, C_A is the feed side VO^{2+} ion concentration, C_B is the permeate side VO^{2+} ion concentration, t is the testing time, A is the effective membrane area, P is the VO^{2+} ion permeability, and L is the membrane thickness.

2.6. Areal specific resistance (ASR) and ionic conductivity

The membrane ASR was measured via the two-probe electrochemical impedance spectroscopy (EIS) method with a Metrohom potentiostat/galvanostat at a frequency range of 10^6 Hz–10 Hz and an amplitude of 10 mV. All the samples were soaked in 1 M H_2SO_4 solution for 1 day and rinsed with DI water for 3 times before the through-plane area resistance measurement. The through-plane cell resistance with (R_{tot}) and without (R_{blank}) membrane was obtained from the high frequency intercept on the Nyquist plot, and the areal resistance of membrane samples was calculated from the difference between these two values (R_{tot}–R_{blank}). The membrane ionic conductivity was calculated from the ASR values.

2.7. Water uptake (WU)

WU (%) was measured according to the difference between the weight of the dry and wet samples as follows:

$$Water\ uptake(WU)(\%) = \frac{(Wwet - Wdry)}{Wdry} \times 100\% \quad (4)$$

where W_{wet} and W_{dry} are the weights of the water-swollen and the corresponding dry membranes, respectively.

2.8. VRFB single cell performance test

The VRFB single cell was assembled as previously reported [32]. The prepared membranes were sandwiched between two graphite felts (MTI, 30 × 30 × 4 mm^3). Two pieces of gold coated copper plates were used as current collector. A bipolar plate (SGL) was placed between current collector and graphite felt. The positive and negative electrolytes contain 1.6 M VO^{2+}/V^{3+} (mol/mol = 1:1) in 4 M H_2SO_4 solution and 1.6 M V^{2+}/V^{3+} in 4.0 M H_2SO_4 solution, respectively. The electrolytes were circulated using peristaltic pumps (Cole-Palmer) at a flow rate of 60 mL/min. The performance of VRFB single cells was measured using a Landt battery testing system (CT2001A-5 V1.8A, 8 Channels). The cut-off voltages for charge and discharge process are 1.65 V and 0.9 V, respectively. The exemplary charge-discharge curve is shown in the supplementary information (Fig. S1). VRFB CE, VE and EE were

Table 2
Properties of the studied AEMs (*p*-TPN1, *m*-TPN1, BPNI-100, and FAP 450) and PEMs (Nafion 117 and 212). Notably, the membrane conductivity was converted from through-plane area resistance values. We believe that, for AEMs, membrane conductivity is mainly contributed by the transport of anions, whereas proton transport is the predominant factor affecting PEM conductivity. In-plane proton conductivity values for Nafions can be found in our previous study [32]. α is the membrane conductivity/VO^{2+} permeability ratio, in units of × 10^{-4} min·S/cm^{-3}.

Samples	Thickness (μm)	WU %	IEC (meq./g)	P_{VO2+} (× 10^{-7} cm^2/min)	Ionic Conductivity at 25 °C (mS/cm)	α	ASR (Ω cm^2)
p-TPN1	35 ± 1	18 ± 1	2.15 ± 0.05	0.74 ± 0.12	12.07 ± 1.96	16.31	0.29 ± 0.03
m-TPN1	35 ± 1	22 ± 1	2.13 ± 0.05	1.26 ± 0.27	12.96 ± 2.78	10.29	0.27 ± 0.05
BPN1-100	45 ± 2	58 ± 1	2.60 ± 0.05	23.83 ± 3.40	20.45 ± 2.91	0.86	0.22 ± 0.06
FAP-450	50 ± 1	9 ± 1	0.93 ± 0.03	7.09 ± 1.10	6.94 ± 1.07	0.98	0.72 ± 0.12
Nafion® 212	55 ± 1	19 ± 1	0.90 ± 0.02	41.21 ± 2.01	23.91 ± 1.17	0.58	0.23 ± 0.05
Nafion® 117	195 ± 1	20 ± 1	0.89 ± 0.02	32.14 ± 1.74	21.91 ± 1.18	0.68	0.89 ± 0.09

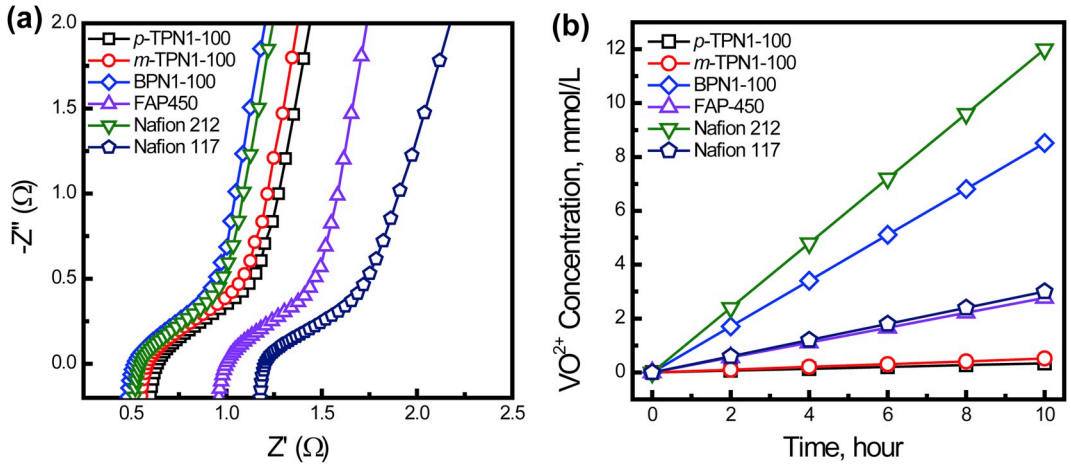

Fig. 2. (a) EIS curves for the area resistance measurement and (b) increase in vanadium ion concentrations during the vanadium ion diffusion tests for different AEMs and PEMs.

calculated with the following equations:

$$Coulombic\ efficiency(CE), \% = \frac{t_{Discharge}}{t_{Charge}} \times 100\% \quad (5)$$

$$Voltage\ efficiency(VE), \% = \frac{V_{Discharge}}{V_{Charge}} \times 100\% \quad (6)$$

$$Energy\ efficiency(EE), \% = \frac{CE \times VE}{100}. \quad (7)$$

2.9. Oxidative stability

The oxidative stability of the membranes was tested according to a method reported in literature [20]. Briefly, the preweighed membranes (0.12 g of dry weight) was immersed in 10 mL of 0.1 M V(V)/4 M H_2SO_4 solutions prepared from the fully charged catholyte solution. The oxidation of membranes leads to the generation of V(IV) species. The concentration of V(IV) species in the solution was monitored using a UV–Vis spectroscopy (T7S, Persee Analytics).

3. Results and discussion

3.1. Membrane characterization

The results of IEC, WU, vanadium permeability (P_{VO2+}), conductivity, and ASR are listed in Table 2. In general, a higher IEC value is required for IEMs to provide satisfactory conductivity. The IEC values of all prepared AEM membranes were in the range of 2.13–2.6 meq./g, which are higher than those of the commercial AEM (0.89 meq./g of FAP450) and PEM (~0.9 meq./g of Nafions). However, the WU values of two terphenyl-based membranes (*p*- and *m*-TPN1) were significantly lower than that of the biphenyl BPN1-100 membrane. We speculate that the lower WU values of the *p*- and *m*-TPN1 membranes might be resulted from the higher hydrophobicity and rigidity of the terphenyl polymer backbone. In general, increasing the WU value of IEMs results in enlarged aqueous channels and greater electrolyte uptake [33,34], which could enhance the transport of charge carriers. However, the increase in ion channel sizes in IEMs also facilitates active species crossover, thus decreasing the selectivity of IEMs (e.g., H^+/VO^{2+}). In addition, membranes with larger WU values usually exhibit poor dimensional stability. Thus, optimization of the WU is required to balance the ion permeance and mechanical properties of a membrane.

As presented in Table 2, the conductivity values of AEMs tended to increase with IEC and WU. However, we also found that the PEMs had higher conductivity values than those of AEMs despite having lower IEC. This finding may have resulted from the intrinsically low mobility of SO_4^{2-} ions (8.27×10^{-8} $m^2s^{-1}V^{-1}$) in aqueous solution, which is approximately one-fourth the mobility of protons [35]. The higher conductivity of BPN1-100 compared with *p*- and *m*- TPN1 may have been a result of both its high WU and IEC, as mentioned above. Of note, however, although conductivity can reflect the ion transport properties of membranes, the voltage efficiency of a battery is more affected by the areal resistance (inverse to ionic conductance), which is a function of membrane thickness. Through optimization of the thickness of the prepared AEMs, the ASR values (0.22–0.29 Ω cm^2) became comparable to that of Nafion® 212 (0.23 Ω cm^2). This result was also evidenced in the overlapping EIS curves of the poly(terphenylene)-based AEMs (*p*-TPN1 and *m*-TPN1) and Nafion® 212 (Fig. 2a). Commercial FAP-450 exhibited a larger ASR (0.72 Ω cm^2) than the prepared AEMs and Nafion® 212, owing to its low IEC value. Nafion® 117 had the largest ASR among all samples, primarily because of its high membrane thickness.

For VRFB applications, vanadium ion permeability is a critical property of IEMs that greatly affects battery performances, such as the CE%, self-discharge rate, and capacity retention. Fig. 2b shows that the vanadium concentrations in the permeant side of the diffusion cell with *p*- and *m*-TPN1 was scarcely noticeable, even after 10 h of measurement, thus implying that the membranes are almost impermeable to VO^{2+} ions. In contrast, the vanadium ion diffusion rates of the Nafion® 212 and BPN1-100 membranes were much higher than those of other membranes. The VO_4^{2+} permeability of *p*- and *m*-TPN1 was an order of magnitude lower than that of commercial PEMs and FAP-450 membrane (Table 2). We calculated the selectivity (α) of membranes by dividing membrane conductivity by the vanadium permeability. A higher selectivity value indicates that a membrane is more likely to transport charge-carrying ions over the active vanadium species. The *p*- and *m*-TPN1 exhibited markedly higher selectivity than Nafion® 117 and 212. For example, the selectivity of the *p*-TPN1 was 28 times higher than that of Nafion® 212. However, BPN1-100, compared with terphenyl AEMs, showed relatively poor selectivity, possibly as a result of wider water channels allowing more vanadium ion crossover. The membrane transport property results suggested that the as-prepared poly-terphenylene AEMs (*p*- and *m*-TPN1 membranes) could provide better battery performance than the commercial Nafion and FAP-450 membranes.

3.2. VRFB single cell performance

3.2.1. VRFB efficiency performance under different current densities

To evaluate the VRFB performance of the membranes, we tested VRFB single cells loaded with all prepared AEM membranes at current

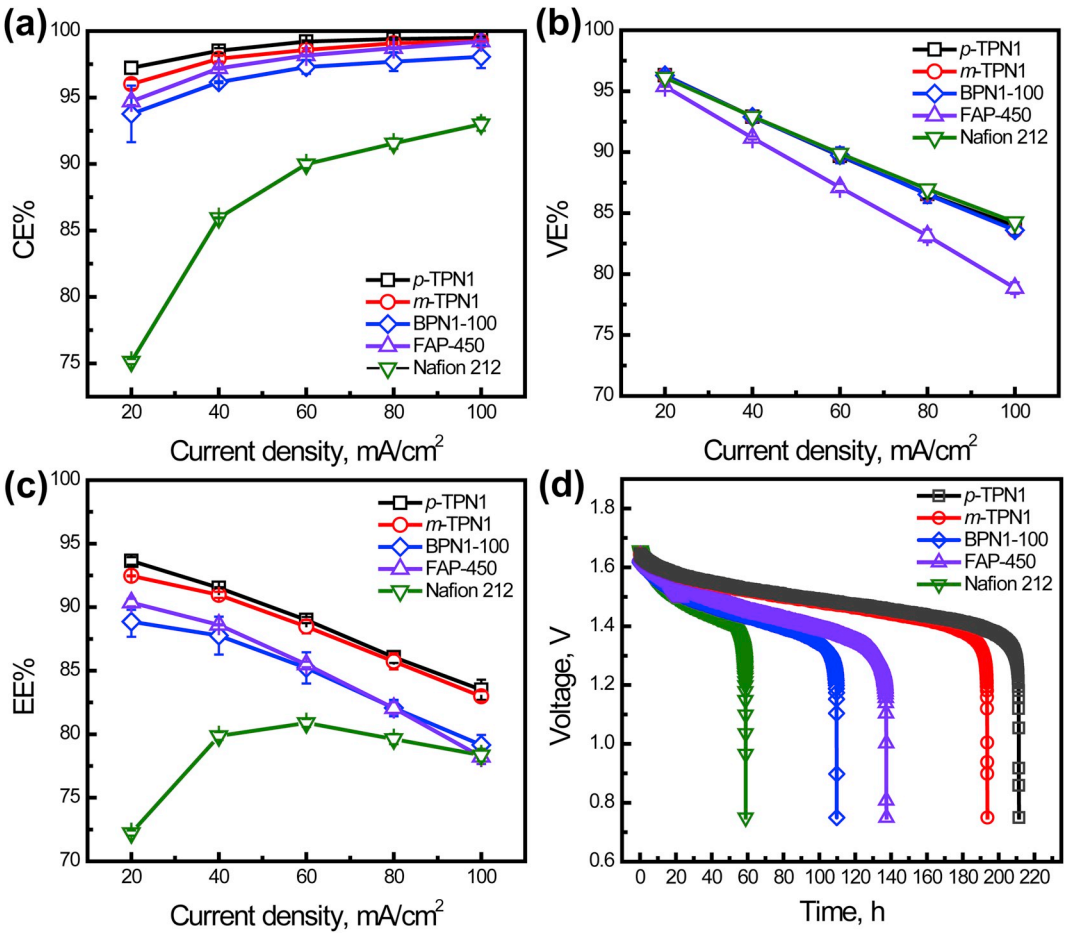

Fig. 3. (a) CE, (b) VE, (c) EE, and (d) self-discharge curves of VRFB single cells with the *p*-TPN1, *m*-TPN1, BPN1-100, and FAP450 membranes at different current densities. Some error bars are hidden by the symbols.

densities ranging from 20 to 100 mA/cm^2 (Fig. 3). Fumasep® FAP-450, a commercial AEM widely used in many VRB applications [36,37], and Nafion® 212 were also evaluated as reference samples. All membranes used in this study had similar thicknesses (35–50 μm), and the data for each current density were averaged from three independent tests.

As depicted in Fig. 3a, the CE values of all tested membranes decreased at lower current densities because of the increased charging/discharging time, which allowed for more active species crossover. In contrast, the VE tended to increase at lower current density because of the reduced ohmic loss. All tested AEMs showed higher CE than that of the proton exchange membrane Nafion® 212. As discussed in the diffusion test results, this finding occurred because the positively charged ion exchange groups in the AEM matrix efficiently repelled the vanadium co-ions, whereas Nafion® 212 allowed transport of positively charged vanadium ions. Among all tested membranes, VRFB with *p*-TPN1 showed the highest CE (~100% at 80 mA/cm^2), followed by the *m*-TPN1 membrane. The high CE values of *p*-TPN1 and *m*-TPN1 membranes were expected because of their extremely low vanadium permeability, as described in Table 2. Especially, *p*-TPN1 showed lower vanadium permeability. This is presumably due to less ordered morphology and less developed ionic clusters of *p*-TPN1 than *m*-TPN1 because of its rigid backbone structure [23]. In addition to the high CE, the *p*- and *m*-TPN1 as well as BPN1-100 membranes also showed excellent VE, even at high current densities (Fig. 3b). We speculate that the high VE values resulted from the synergistic contribution of high ion exchange capacity and the favorable hydrophobic−hydrophilic domains that facilitate anion transfer [23]. As shown in Fig. 3c, owing to both high CE and VE, the *p*- and *m*-TPN1 exhibited excellent EE, which is the product of CE and VE. In particular, *p*-TPN1 showed the best overall performance among all tested membranes. The highest EE value of 93.64% was achieved at the current density of 20 mA/cm^2. This EE value of the *p*-TPN1 outperformed that of the PEMs and AEMs reported in literatures (Supplementary Table S1). The commercial FAP-450 also showed good CE. However, owing to the high ASR, its VE was lower than that of other membranes, thus leading to a lower overall EE. Compared with AEMs, commercial PEMs and Nafion® 212, provide satisfactory VE but low CE and EE, especially at low current densities, because of the faster cation permeation across Nafion membranes.

Another criterion for high-performance membrane separators in VRFB is a slow self-discharge rate. To evaluate the self-discharge performance of the AEMs and PEM, we self-discharged battery single cells loaded with various membranes to 0.8 V. As shown in Fig. 3d, the open circuit voltage of batteries with all membranes decreased gradually over the self-discharging, mainly because of crossover flux of the vanadium ions. At the end of each test, the open circuit voltage sharply decreased to less than 1 V. During the self-discharge measurement, the diffusion of vanadium ions was the major factor accounting for the active species crossover. As a result, the trend observed for the self-discharge time was in good accordance with the results of vanadium permeation tests for the membranes. At the cut-off voltage of 0.8 V, the self-discharge times of Nafion® 212, BPN1-100, FAP 450, *m*-TPN1, and *p*-TPN1 were 58.7, 109.9, 137.2, 193.7, and 211.3 h, respectively. Among all the membranes, *p*-TPN1 membrane exhibited the longest self-discharge time (approximately 10 days). This superior performance of *p*-TPN1 further demonstrated its excellent ability to reject vanadium species, a property that is beneficial to extending the stand-by time of VRFB stacks.

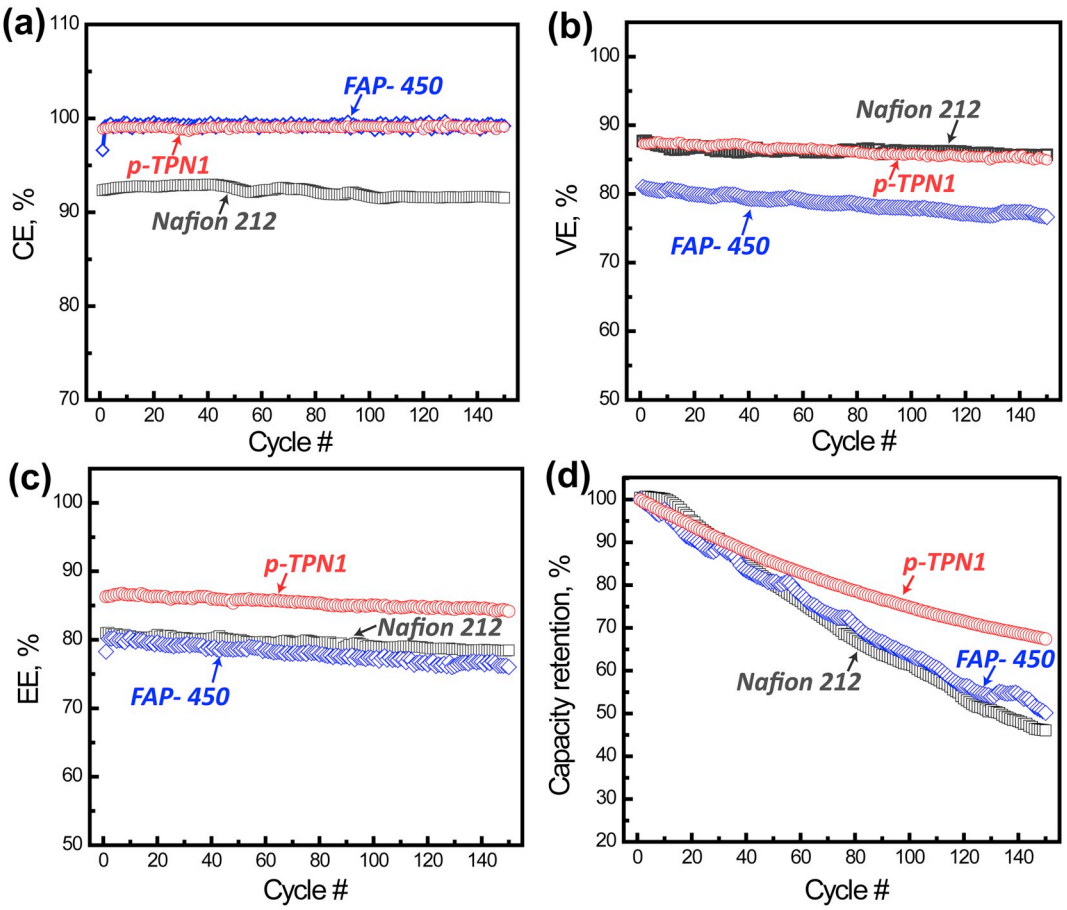

Fig. 4. 1–150 cycles of VRFB single cell performance in terms of a. CE %, b. VE %, c. EE, and d. capacity decay curves with *p*-TPN1, Nafion 212, and FAP 450 membrane.

3.2.2. Stability of membranes in VRFB

Long-term VRFB cycle stability testing with the *p*-TPN1 membrane, which showed the best performance among the as-prepared AEMs, was performed for 150 cycles. For comparison, we also tested Fumasep® FAP-450 AEM and Nafion® 212 at a current density of 80 mA/cm^2. As shown in Fig. 4a, the CE of the *p*-TPN1 membrane was stable at ~100% over the course of the testing, and the VE and EE also remained high (>85%). In comparison, although Nafion® 212 also showed stable performance, its CE (92%) and EE (80%) were lower than those of *p*-TPN1 (Fig. 4 **a and c**). Fumasep® FAP-450 showed a stable CE value similar to that of *p*-TPN1. However, its VE was approximately 7–8% lower than that of *p*-TPN1, owing to its high membrane resistance. In addition, FAP-450 showed relatively less stable VE and EE than Nafion and *p*-TPN1.

In Fig. 4d, the capacity retention of VRFB single cell *p*-TPN1, Fumasep® FAP-450 and Nafion® 212 is plotted against cycle numbers. A higher capacity retention was found for of *p*-TPN1 than Nafion® 212 and FAP-450. The capacity loss per cycle for *p*-TPN1 was approximately 0.2%, whereas Nafion® 212 and FAP-450 exhibited capacity losses of 0.35% and 0.33% per cycle, respectively. The faster capacity decay of Nafion® 212 and FAP-450 may have been a consequence of the faster crossover of vanadium ions. Besides the superior cycle stability and high capacity retention, *p*-TPN1 also exhibits good chemical stability in the oxidative V(V) solution, which is close to the stability of commercial Fumasep® FAP-450 and Nafion 212 membranes (Fig. S2). The stability tests result demonstrated great potential of *p*-TPN1 membranes for long-term operation in VRFB applications.

4. Conclusion

A series of poly(terphenylene) and biphenyl-based anion exchange membranes were fabricated and optimized for VRFB applications. These membranes exhibited both low vanadium ion crossover and low membrane resistance, owing to their well-balanced ion channel structure and functionalities. Consequently, the ion selectivity of the terphenylene-based *p*- and *m*-TPN1 membranes outperformed Nafion by 28 and 18 times, respectively. Superior VRFB single cell performance was further obtained with the prepared poly(terphenylene)-based AEMs. Among all membranes tested, *p*-TPN1 exhibited the highest overall performance at all current densities. In addition, VRFB cell cycle stability testing with *p*-TPN1 for 150 cycles showed a highly stable CE (>99%) and slow capacity decay. The results indicate that these poly(terphenylene)-based AEMs are promising candidates for development of high performance VRFBs.

Declaration of competing interest

The authors declare that they have no known competing financial interests or personal relationships that could have appeared to influence the work reported in this paper.

Acknowledgements

This work was supported by grants from the National Science Foundation (grant No. CBET-1706910), the U.S. Department of Energy, Office of Energy Efficiency and Renewable Energy (EERE), Fuel Cell Technology Office (FCTO; with Dr. Nancy Garland and Dr. David

Peterson as program managers), ARPA-E (IONICS DE-AR0000769 and REFUEL DE-AR0000805), and New York State Energy Research and Development Authority (NYSERDA; grant No. 127734). T. Wang acknowledges support from the UIC Provost's Graduate Research Award program. S. Kim and C. Bae thank StorEn for discussions.

Appendix A. Supplementary data

Supplementary data to this article can be found online at https://doi.org/10.1016/j.memsci.2019.117665.

References

[1] B. Dunn, H. Kamath, J.-M. Tarascon, Electrical energy storage for the grid: a battery of choices, Science 334 (2011) 928–935.
[2] G.L. Soloveichik, Battery technologies for large-scale stationary energy storage, Annu. Rev. Chem. Biomol. Eng 2 (2011) 503–527.
[3] M. Rychcik, M. Skyllas-Kazacos, Characteristics of a new all-vanadium redox flow battery, J. Power Sources 22 (1988) 59–67.
[4] G. Kear, A.A. Shah, F.C. Walsh, Development of the all-vanadium redox flow battery for energy storage: a review of technological, financial and policy aspects, Int. J. Energy Res. 36 (2012) 1105–1120.
[5] B. Schwenzer, J. Zhang, S. Kim, L. Li, J. Liu, Z. Yang, Membrane development for vanadium redox flow batteries, ChemSusChem 4 (2011) 1388–1406.
[6] X. Li, H. Zhang, Z. Mai, H. Zhang, I. Vankelecom, Ion exchange membranes for vanadium redox flow battery (VRB) applications, Energy Environ. Sci. 4 (2011) 1147–1160.
[7] T.K. Hoang, P. Chen, Recent development of polymer membranes as separators for all-vanadium redox flow batteries, RSC Adv. 5 (2015) 72805–72815.
[8] S. Winardi, S.C. Raghu, M.O. Oo, Q. Yan, N. Wai, T.M. Lim, M. Skyllas-Kazacos, Sulfonated poly (ether ether ketone)-based proton exchange membranes for vanadium redox battery applications, J. Membr. Sci. 450 (2014) 313–322.
[9] C. Sun, J. Chen, H. Zhang, X. Han, Q. Luo, Investigations on transfer of water and vanadium ions across Nafion membrane in an operating vanadium redox flow battery, J. Power Sources 195 (2010) 890–897.
[10] D. Chen, S. Wang, M. Xiao, D. Han, Y. Meng, Sulfonated poly (fluorenyl ether ketone) membrane with embedded silica rich layer and enhanced proton selectivity for vanadium redox flow battery, J. Power Sources 195 (2010) 7701–7708.
[11] J.J. Min-suk, J. Parrondo, C.G. Arges, V. Ramani, Polysulfone-based anion exchange membranes demonstrate excellent chemical stability and performance for the all-vanadium redox flow battery, J. Mater. Chem. A 1 (2013) 10458–10464.
[12] J. Zeng, C. Jiang, Y. Wang, J. Chen, S. Zhu, B. Zhao, R. Wang, Studies on polypyrrole modified nafion membrane for vanadium redox flow battery, Electrochem. Commun. 10 (2008) 372–375.
[13] X. Teng, J. Dai, J. Su, G. Yin, Modification of Nafion membrane using fluorocarbon surfactant for all vanadium redox flow battery, J. Membr. Sci. 476 (2015) 20–29.
[14] S. Lu, C. Wu, D. Liang, Q. Tan, Y. Xiang, Layer-by-layer self-assembly of Nafion–[CS–PWA] composite membranes with suppressed vanadium ion crossover for vanadium redox flow battery applications, RSC Adv. 4 (2014) 24831–24837.
[15] L. Yu, F. Lin, L. Xu, J. Xi, A recast Nafion/graphene oxide composite membrane for advanced vanadium redox flow batteries, RSC Adv. 6 (2016) 3756–3763.
[16] Q. Luo, H. Zhang, J. Chen, P. Qian, Y. Zhai, Modification of Nafion membrane using interfacial polymerization for vanadium redox flow battery applications, J. Membr. Sci. 311 (2008) 98–103.
[17] H. Prifti, A. Parasuraman, S. Winardi, T.M. Lim, M. Skyllas-Kazacos, Membranes for redox flow battery applications, Membranes 2 (2012) 275–306.
[18] D. Chen, M.A. Hickner, E. Agar, E.C. Kumbur, Selective anion exchange membranes for high coulombic efficiency vanadium redox flow batteries, Electrochem. Commun. 26 (2013) 37–40.
[19] D. Chen, M.A. Hickner, Degradation of imidazolium-and quaternary ammonium-functionalized poly (fluorenyl ether ketone sulfone) anion exchange membranes, ACS Appl. Mater. Interfaces 4 (2012) 5775–5781.
[20] T. Mohammadi, M.S. Kazacos, Evaluation of the chemical stability of some membranes in vanadium solution, J. Appl. Electrochem. 27 (1997) 153–160.
[21] H.-S. Dang, E.A. Weiber, P. Jannasch, Poly (phenylene oxide) functionalized with quaternary ammonium groups via flexible alkyl spacers for high-performance anion exchange membranes, J. Mater. Chem. A 3 (2015) 5280–5284.
[22] Y. Li, X. Lin, L. Wu, C. Jiang, M.M. Hossain, T. Xu, Quaternized membranes bearing zwitterionic groups for vanadium redox flow battery through a green route, J. Membr. Sci. 483 (2015) 60–69.
[23] W.-H. Lee, E.J. Park, J. Han, D.W. Shin, Y.S. Kim, C. Bae, Poly (terphenylene) anion exchange membranes: the effect of backbone structure on morphology and membrane property, ACS Macro Lett. 6 (2017) 566–570.
[24] W.-H. Lee, Y.S. Kim, C. Bae, Robust hydroxide ion conducting poly (biphenyl alkylene) s for alkaline fuel cell membranes, ACS Macro Lett. 4 (2015) 814–818.
[25] W.-H. Lee, Y.S. Kim, C. Bae, Robust hydroxide ion conducting poly(biphenyl alkylene)s for alkaline fuel cell membranes, ACS Macro Lett. 4 (2015) 814–818.
[26] F. Huang, L. Hou, H. Wu, X. Wang, H. Shen, W. Cao, W. Yang, Y. Cao, High-efficiency, environment-friendly electroluminescent polymers with stable high work function metal as a Cathode: green- and yellow-emitting conjugated polyfluorene polyelectrolytes and their neutral precursors, J. Am. Chem. Soc. 126 (2004) 9845–9853.
[27] B. Jiang, L. Wu, L. Yu, X. Qiu, J. Xi, A comparative study of Nafion series membranes for vanadium redox flow batteries, J. Membr. Sci. 510 (2016) 18–26.
[28] H.-Y. Jung, S. Jeong, Y. Kwon, The effects of different thick sulfonated poly (ether ether ketone) membranes on performance of vanadium redox flow battery, J. Electrochem. Soc. 163 (2016) A5090–A5096.
[29] X. Teng, Y. Zhao, J. Xi, Z. Wu, X. Qiu, L. Chen, Nafion/organically modified silicate hybrids membrane for vanadium redox flow battery, J. Power Sources 189 (2009) 1240–1246.
[30] X. Luo, Z. Lu, J. Xi, Z. Wu, W. Zhu, L. Chen, X. Qiu, Influences of permeation of vanadium ions through PVDF-g-PSSA membranes on performances of vanadium redox flow batteries, J. Phys. Chem. B 109 (2005) 20310–20314.
[31] J. Xi, Z. Wu, X. Qiu, L. Chen, Nafion/SiO2 hybrid membrane for vanadium redox flow battery, J. Power Sources 166 (2007) 531–536.
[32] T. Wang, S.J. Moon, D.-S. Hwang, H. Park, J. Lee, S. Kim, Y.M. Lee, S. Kim, Selective ion transport for a vanadium redox flow battery (VRFB) in nano-crack regulated proton exchange membranes, J. Membr. Sci. 583 (2019) 16–22.
[33] H.G. Kim, R. Kim, S. Kim, C. Choi, B. Kim, H. Guim, H.-T. Kim, Propylene carbonate-derived size modulation of water cluster in pore-filled Nafion/polypropylene composite membrane for the use in vanadium redox flow batteries, J. Ind. Eng. Chem. 60 (2018) 401–406.
[34] M.S. Cha, J.Y. Lee, T.-H. Kim, H.Y. Jeong, H.Y. Shin, S.-G. Oh, Y.T. Hong, Preparation and characterization of crosslinked anion exchange membrane (AEM) materials with poly (phenylene ether)-based short hydrophilic block for use in electrochemical applications, J. Membr. Sci. 530 (2017) 73–83.
[35] J. Si, Y. Lv, S. Lu, Y. Xiang, Microscopic phase-segregated quaternary ammonia polysulfone membrane for vanadium redox flow batteries, J. Power Sources 428 (2019) 88–92.
[36] D. Zhang, X. Yan, G. He, L. Zhang, X. Liu, F. Zhang, M. Hu, Y. Dai, S. Peng, An integrally thin skinned asymmetric architecture design for advanced anion exchange membranes for vanadium flow batteries, J. Mater. Chem. A 3 (2015) 16948–16952.
[37] S. Peng, X. Yan, D. Zhang, X. Wu, Y. Luo, G. He, AH 3 PO 4 preswelling strategy to enhance the proton conductivity of a H 2 SO 4-doped polybenzimidazole membrane for vanadium flow batteries, RSC Adv. 6 (2016) 23479–23488.